PanVasc: A Shape-Aware Framework for Peripancreatic Vascular Invasion Assessment in Pancreatic Ductal Adenocarcinoma

Muhammad Ibtsaam Qadir[1 [0009−0002−5521−2855]], Alexa J. Hughes[2 [0000−0002−2972−1253]], Ryan J. Ellis[2 [0000−0003−2637−9445]], and Fiona R. Kolbinger[1,2,3,4 [0000−0003−2265−4809]]

[1] Weldon School of Biomedical Engineering, Purdue University, West Lafayette, IN, USA

[2] Department of Surgery, Indiana University School of Medicine, Surgical Outcomes and Quality Improvement Center (SOQIC), Indianapolis, IN, USA

[3] Department of Visceral, Thoracic and Vascular Surgery, Medical Faculty and University Hospital Dresden, TUD Dresden University of Technology, Dresden, Germany

[4] Else Kröner Fresenius Center for Digital Health, Medical Faculty and University Hospital Dresden, TUD Dresden University of Technology, Dresden, Germany

{mqadir,fkolbing}@purdue.edu

Abstract. Assessment of pancreatic ductal adenocarcinoma (PDAC) resectability relies on the spatial relationship between the tumor and peripancreatic vessels. Current evaluation reduces a complex 3D interface to vessel encasement angles measured on selected 2D CT slices. We introduce *PanVasc*, a shape-based framework for continuous and branch-aware quantification of tumor-vessel involvement. First, vessel surfaces are encoded with a pointwise tumor-proximity field defined by the distance to the nearest tumor-surface point. Second, each vessel is decomposed into branches and represented by a spline centerline with a rotation-minimizing local reference frame. Tumor contact is then measured circumferentially at regularly sampled centerline locations. This results in continuous encasement-angle profile $A(s)$ along each branch. Third, the profiles are summarized using the peak encasement angle $E_{\max}$ and area under the encasement curve (AUEC) to capture the maximum tumor encasement and its longitudinal extent. A 3D nnU-Net trained on 1,024 annotated CT volumes was used to segment the tumor and peripancreatic vasculature. PanVasc was evaluated on an independent cohort of 364 patients with resected PDAC and preoperative resectability labels determined via the traditional technique in routine clinical care. Across resectable ($n = 266$), borderline-resectable ($n = 78$), and locally advanced ($n = 20$) disease, arterial $E_{\max}$ and AUEC increased monotonically with resectability stage (Jonckheere–Terpstra $p < 0.05$), with Spearman correlations reaching $\rho = 0.26$. PanVasc provides an interpretable geometric representation of the complete tumor-vessel interface and enables reproducible, continuous quantification of vascular involvement from segmentation masks.

Keywords: Vascular encasement quantification · 3D vessels · Encasement profiles · Shape-aware surgical planning · Pancreatic cancer.

1 Introduction

Pancreatic ductal adenocarcinoma (PDAC) remains among the most lethal solid tumors, with a five-year survival of under 15% [5]. Complete surgical resection is the only treatment offering a chance of cure, yet only about 15–20% of patients present with anatomically resectable disease [14]. Pancreatic surgery carries substantial morbidity including postoperative pancreatic fistula, delayed gastric emptying, and hemorrhage [11], and its oncologic benefit depends heavily on the completeness of tumor resection. A microscopically positive (R1) margin, i.e., microscopically detectable remaining tumor, is consistently associated with earlier recurrence and shorter survival compared to patients with complete (R0) resection. The patients who fail to achieve complete resection frequently endure prolonged recovery and complications that delay or preclude adjuvant therapy [1, 3]. Given the high risk of complications and association of vascular invasion with worse prognosis, improving preoperative selection and surgical planning is important for optimal decision making.

Preoperative resectability is currently estimated from cross-sectional computed tomography (CT) images, with each tumor assigned to one of four categories i.e., resectable, borderline resectable, locally advanced, or metastatic (and hence, unresectable), based on clinical treatment guidelines such as those of the National Comprehensive Cancer Network (NCCN) [15]. According to these guidelines, the preoperative resectability status is based on the relationship between the tumor and the peripancreatic vasculature: the degree of circumferential contact with the celiac axis (CA), superior mesenteric artery (SMA), common hepatic artery, and the superior mesenteric and portal veins (SMV/PV). A 180° of contact serves as a threshold separating abutment ($<$180°) from encasement ($>$180°) [15, 2]. Borderline-resectable generally involves limited arterial contact of ($\leq$ 180°) or reconstructible venous involvement, whereas locally advanced disease is characterized by arterial encasement of ($>$ 180°) or unreconstructible vascular involvement [15]. In practice, radiologists and surgeons assess this relationship using axial images and multiplanar reconstructions oriented perpendicular to the vessel, integrating multiple 2D views to infer the 3D tumor-vessel interface. This is a task that is cognitively demanding, requires considerable experience, and lacks reproducibility [8, 4]. A continuous geometric relationship is thereby compressed into a coarse categorical label. Moreover, most of the information that distinguishes one borderline resectable tumor from another, i.e., where around the vessel the tumor sits, over how long a segment, and how that pattern is distributed across several vessels, is never made explicit or measured.

Recent work has sought to make this geometry quantitative. Radiomic models built from the tumor and perivascular tissue improve prediction of SMA margin status and resectability over standard interpretation [19, 18]. Most directly, interface-severity grading has shown that combining a circumferential contact

angle with a contact length stratifies survival preoperatively [9]. Together, these establish that both the tumor–vessel contact angle and its longitudinal extent carry surgical and prognostic signal. However, in these studies, the contact angle is typically read on a single representative axial slice and is measured in the image plane rather than on the true vessel surface. This technically ignores varying caliber, eccentric lumens, and oblique vessel orientation. Hence, the resulting descriptors are often texture features rather than interpretable geometry a surgeon can reason about and will recognize intraoperatively. None of these methods interpret the full interface in a form that is at once continuous and reproducible.

We address this gap with a shape-based framework that converts the segmented tumor and peripancreatic vessels into explicit, quantitative descriptions of their spatial relationship. Our contributions are threefold:

1. First, we render a 3D tumor-proximity map i.e., the vessel surface colored by distance to the nearest tumor-surface point. This provides a clinician with an immediate, view-independent picture of where each vessel is in contact with or in proximity to the tumor.
2. Second, we reduce this surface field to an encasement profile. We represent the circumferential angle of tumor contact as a continuous function of tumor position along each vessel or vascular branch. This is computed on the true vessel surface using a rotation-minimizing frame and explicit handling of vascular branching.
3. Third, we summarize each profile by the area under the encasement curve and peak encasement angle, two scalars that capture how much of the vessel is contacted and how tightly. This provides candidate interpretable preoperative markers to support surgical planning.

2 Methods

2.1 Tumor-Vessel Proximity Heatmap for Peripancreatic Vascular Invasion Assessment

To spatially assess and visualize the tumor–vessel interface and invasion, the framework generates a 3D surface representation of each peripancreatic vessel (SMA, CA, and veins [SMV and PV]) and encodes the pointwise distance to the tumor surface as a continuous map. This produces a view-independent tumor–vessel proximity map.

Surface extraction. We use the multi-label segmentation with voxel-to-world affine $A \in \mathbb{R}^{4\times4}$. Anisotropic voxel spacing is recovered from the linear part of the affine as column norms $s_k = \left\|A_{1:3,\,k}\right\|_2, k \in \{1,2,3\}$ so that all geometry is expressed in millimeters. For a structure with binary mask M we zero-pad M by two voxels for a closed, watertight boundary at the volume edges and extract the 0.5-isosurface of the trilinearly interpolated indicator f,

$$\mathcal{S} = \{\, x \in \mathbb{R}^3 : f(x) = \tfrac{1}{2} \,\}, \tag{1}$$

using the marching-cubes algorithm [13] with spacing s. This results in a triangle mesh (V, F) whose vertices are then shifted by $-2s$ to undo the padding. Because the affine of a CT acquisition is shear-free, embedding the voxel grid with the diagonal spacing $\mathrm{diag}(s)$ is an isometry of the full affine, i.e., all inter-vertex Euclidean distances are preserved exactly, so the proximity field below is metrically correct even though absolute orientation is not retained. Marching-cubes surfaces exhibit terraced voxel artifacts. Therefore, Taubin's $\lambda\,|\,\mu$ low-pass filter is applied [16], which alternates a smoothing step with positive and negative scale factors to suppress the staircasing effect without the volumetric shrinkage of repeated Laplacian smoothing. With the umbrella operator

$$\mathcal{L}(v_i) = \frac{1}{|\mathcal{N}(i)|} \sum_{j \in \mathcal{N}(i)} (v_j - v_i), \tag{2}$$

each iteration performs $v_i \leftarrow v_i + \lambda\,\mathcal{L}(v_i)$ followed by $v_i \leftarrow v_i + \mu\,\mathcal{L}(v_i)$ with $0 < \lambda < -\mu$, run for 80 iterations at a pass-band of 0.05. Sensitivity of the tumor-proximity map to the Taubin smoothing parameters ($N_{iteration}$ and *pass-band*) is shown in Supplementary Figure 1.

Proximity field. Let T denote the tumor surface and $\mathcal{V}_\ell$ a vessel surface, both obtained as above. To reduce the discretization bias of a vertex-to-vertex query, the tumor surface is first refined by two iterations of interpolating (butterfly) subdivision. This inserts new vertices on edges while leaving the original vertices in place and produces a dense sample V_T^* of ∂T. For every vessel vertex $v \in V_{\mathcal{V}_\ell}$ we assign the Euclidean nearest-neighbor distance to this sample,

$$d(v) = \min_{p \in V_T^*} \|v - p\|_2 \;\approx\; \min_{p \in \partial T} \|v - p\|_2, \tag{3}$$

computed with a k-d tree, and clamp it to a fixed range

$$\hat{d}(v) = \min\big(d(v),\, d_{\max}\big), \qquad d_{\max} = 50 \text{ mm}, \tag{4}$$

where $d_{\max}$ is a visualization parameter that caps distances beyond clinical interest. It only affects the color mapping and not the derived measures (sensitivity analysis in Supplementary Figure 2). The scalar field $\hat{d}$ is stored on the mesh and mapped to a color map normalized to $[0, d_{\max}]$, with low values (vessel-tumor contact) at the warm end. The field is unsigned i.e., the vessels lie outside the tumor, so contact corresponds to $\hat{d} \to 0$.

2.2 Continuous Encasement Angle Profile

The continuous encasement angle profile represents the circumferential extent of tumor contact measured on true vessel surface as a function of position along each vessel.

Algorithm 1 Tumor-vessel proximity maps

Require: Label volume S, affine matrix A, vessel labels $\mathcal{L}$, tumor label ℓ_T, and distance cap $d_{\max}$
Ensure: Vessel surfaces $\{\mathcal{V}_\ell\}$ with vertex-wise proximity values $\hat{d}$

$s \leftarrow \textsc{VoxelSpacing}(A)$ ▷ $s_k = \|A_{1:3,k}\|_2$ in mm
$T \leftarrow \textsc{MaskToMesh}(\mathbf{1}[S = \ell_T], s)$
$T^* \leftarrow \textsc{Subdivide}(T, 2)$ ▷ Butterfly subdivision
$\mathcal{K} \leftarrow \text{KDTree}(V(T^*))$
for all $\ell \in \mathcal{L}$ **do**
  if $|\{x : S(x) = \ell\}| > 0$ **then**
    $\mathcal{V}_\ell \leftarrow \textsc{MaskToMesh}(\mathbf{1}[S = \ell], s)$
    for all $v \in V(\mathcal{V}_\ell)$ **do**
      $d(v) \leftarrow \textsc{NearestDistance}(\mathcal{K}, v)$
      $\hat{d}(v) \leftarrow \min(d(v), d_{\max})$
    end for
    Attach $\hat{d}$ to $\mathcal{V}_\ell$ as a vertex-wise scalar field
  end if
end for
return $\{\mathcal{V}_\ell\}_{\ell \in \mathcal{L}}$

function $\textsc{MaskToMesh}(M, s)$
  $\widetilde{M} \leftarrow \textsc{Pad}(M, 2)$
  $(V, F) \leftarrow \textsc{MarchingCubes}(\widetilde{M}, 0.5, s)$
  $V \leftarrow V - 2s$ ▷ Remove padding offset in physical space
  $(V, F) \leftarrow \textsc{CleanTriangulate}(V, F)$
  $V \leftarrow \textsc{TaubinSmooth}(V, F, 80, 0.05)$
  $(V, F) \leftarrow \textsc{ComputeNormals}(V, F)$
  return (V, F)
end function

Surface distance field. As in the tumor proximity heatmap, we extract the vessel surface by marching cubes and express its vertices $V = \{\mathbf{v}_i\}$ in world millimeters. Each vertex is equipped with its Euclidean distance to the tumor surface $\partial\mathcal{T}$, evaluated with a k-d tree over the tumor boundary points. This is the same scalar which here is used to drive the contact measurement.

Branch centerline and arc length. A 3-D skeleton of the vessel mask is obtained by homotopic thinning and converted to a graph. The graph is reduced to a tree and short spurious twigs ($\leq 5mm$) are pruned, as these short segments can arise from skeletonization artifacts and fall below the scale at which resectability is graded. The tree is then split at bifurcations (degree ≥ 3) into individual branches. Each branch polyline is fitted with a smoothing spline $\mathbf{c}(s)$, resampled to n_s stations, and parameterized by arc length $s \in [0, L]$, with unit tangent $\mathbf{T}(s) = \mathbf{c}'(s)/\|\mathbf{c}'(s)\|$. Branches shorter than $L_{\min}$ are discarded (default $10mm$), as these typically correspond to small-caliber vessels approaching the imaging resolution and are of limited clinical relevance.

Around each centerline, we attach a circumferential angle through a rotation-minimizing frame $(\mathbf{T}, \mathbf{N}, \mathbf{B})$, which transports the cross-section along the branch without spurious twist. The frame is seeded at the first station by taking $\mathbf{N}_0$ as a fixed reference axis projected onto the plane orthogonal to $\mathbf{T}_0$ and normalized (the reference is switched if near-parallel to $\mathbf{T}_0$), with $\mathbf{B}_0 = \mathbf{T}_0 \times \mathbf{N}_0$. This seed fixes only the origin $\theta = 0$ of the angular coordinate and does not affect the encasement angle defined below. The normal is propagated by the minimal rotation that aligns successive tangents,

$$\mathbf{N}_i = \mathcal{R}(\mathbf{T}_{i-1} \to \mathbf{T}_i)\, \mathbf{N}_{i-1}, \qquad \mathbf{B}_i = \mathbf{T}_i \times \mathbf{N}_i. \tag{5}$$

Each vessel vertex $\mathbf{v}$ is assigned to its nearest station $i^\star(\mathbf{v}) = \arg\min_i \|\mathbf{v} - \mathbf{c}(s_i)\|$, and its angular position is read off in that frame,

$$\theta(\mathbf{v}) = \operatorname{atan2}\big(\mathbf{w}\cdot\mathbf{B}_{i^\star},\ \mathbf{w}\cdot\mathbf{N}_{i^\star}\big), \qquad \mathbf{w} = \mathbf{v} - \mathbf{c}(s_{i^\star}). \tag{6}$$

Vertices are binned onto an $n_s \times n_\theta$ grid. Each bin stores the minimum tumor distance among its vertices, $D(s_i, \theta_j) = \min_{\mathbf{v} \in \mathrm{bin}(i,j)} d(\mathbf{v})$.

Encasement angle. A surface patch is in contact with the tumor when it is within a threshold τ. The encasement angle at the station s_i is the angular measure of the circumference contacted,

$$A(s_i) = \sum_{j=1}^{n_\theta} \mathbf{1}\big[D(s_i, \theta_j) \le \tau\big]\, \Delta\theta, \qquad \Delta\theta = \frac{2\pi}{n_\theta}, \tag{7}$$

reported in degrees. Stations within approximately one local vessel radius of a bifurcation are excluded, as the circular cross-section is ill-defined there and would otherwise register a spurious full encasement. The per-vessel summary is the peak of the profile,

$$E_{\max} = \max_i A(s_i), \tag{8}$$

read against reference lines at 180° (the NCCN abutment/encasement threshold) and 270° (high-grade encasement). The profile $A(s)$ against arc length s is the output of this tool. We use $\tau = 2$ mm, $n_\theta = 180$ (resulting in 2° in angular resolution so that contact thresholds 180° and 270° fall on bin boundary), and $n_s = 160$ (sub-voxel longitudinal spacing) throughout.

2.3 Area Under the Encasement Curve (AUEC)

The encasement-angle profile $A(s)$ reduces the full tumor-vessel interface to a curve, which is then integrated to quantify how tightly and how far the tumor wraps a vessel. The resulting scalar is referred to as AUEC. For a vessel branch b of length L_b, AUEC is the integral of the angle profile along the branch,

$$\mathrm{AUEC}_b = \int_0^{L_b} A(s)\, ds \ \approx\ \sum_i A(s_i)\, \Delta s_i, \tag{9}$$

Algorithm 2 Continuous encasement-angle profile

Require: Vessel mask M, tumor surface $\partial\mathcal{T}$, affine A; contact threshold τ, bins n_θ, stations n_s, min. length $L_{\min}$
Ensure: Encasement profiles $\{A_b(s)\}$ over branches b

$V \leftarrow \textsc{VesselSurface}(M, A)$ ▷ marching cubes, world mm
for all $\mathbf{v} \in V$ **do**
  $d(\mathbf{v}) \leftarrow \min_{\mathbf{q}\in\partial\mathcal{T}} \|\mathbf{v} - \mathbf{q}\|_2$ ▷ k-d tree query
end for
$\mathcal{B} \leftarrow \textsc{SkeletonBranches}(M)$ ▷ thinning → tree → split at bifurcations
for all $b \in \mathcal{B}$ **do**
  if $\text{length}(b) \geq L_{\min}$ **then**
    $(\mathbf{c}, \mathbf{T}, s) \leftarrow \textsc{FitCentreline}(b, n_s)$ ▷ spline, arc length
    $(\mathbf{N}, \mathbf{B}) \leftarrow \textsc{MinRotationFrame}(\mathbf{T})$
    $D \leftarrow +\infty^{\,n_s \times n_\theta}$
    for all $\mathbf{v} \in V$ assigned to b **do**
      $i \leftarrow \arg\min_i \|\mathbf{v} - \mathbf{c}(s_i)\|$
      $\mathbf{w} \leftarrow \mathbf{v} - \mathbf{c}(s_i)$
      $\theta \leftarrow \text{atan2}(\mathbf{w}\cdot\mathbf{B}_i,\ \mathbf{w}\cdot\mathbf{N}_i)$
      $j \leftarrow \lfloor \theta\, n_\theta / 2\pi \rfloor$
      $D_{ij} \leftarrow \min(D_{ij},\, d(\mathbf{v}))$
    end for
    for $i \leftarrow 1$ to n_s **do**
      $A_b(s_i) \leftarrow \dfrac{2\pi}{n_\theta} \sum_j \mathbf{1}[D_{ij} \leq \tau]$ ▷ degrees; undefined near junctions
    end for
    $E^b_{\max} \leftarrow \max_i A_b(s_i)$
  end if
end for
return $\{A_b(s)\}$

evaluated by the trapezoidal rule over the arc-length stations s_i (units: degree-millimeters). Junction-clipped stations contribute zero, so the confluence shared between branches is not double-counted. The skeleton splits a vessel into branches at its bifurcations, so a vessel's total involvement is the sum over its branches,

$$\text{AUEC}_v = \sum_{b\in v} \text{AUEC}_b, \tag{10}$$

treating each anatomical vessel v as one structure. This results in a single value per vessel per patient.

3 Experimental Setup

Datasets. For the implementation and validation of this framework, we used two cohorts. *PanTS* is a large-scale public dataset of abdominal CT with voxel-level annotations of the pancreatic tumor and peripancreatic vasculature [12]. From its 9,901 volumes we retained all tumor-bearing cases and excluded volumes

with non-orthogonal acquisition geometry or label-image orientation mismatch. This resulted in 1,024 annotated volumes used to develop the segmentation model. The *Indiana University Health (IUH)* cohort is a single-center, retrospective set of 364 patients who underwent partial pancreatectomy for PDAC between 2015 and 2024, with preoperative CT, resectability classification, and other clinical (e.g., demographic) data. This data had no expert segmentations. PanTS supplies the labels to train segmentation and IUH supplies an independent clinical cohort on which the shape metrics i.e., AUEC and E_{max}axare evaluated against resectability. The segmentation test set and the IUH cohort are disjoint. The overall analysis was reviewed and approved by the institutional review board at Purdue University (IRB #`2023-1736`, approval date: February 7, 2024).

Segmentation. We trained a single 3D full-resolution nnU-Net [6] for 1,000 epochs to segment the following structures: pancreatic tumor, pancreatic head, pancreatic body, pancreatic tail, SMA, CA, and regional veins, on an NVIDIA L40 GPU. From the 1,024 CT volumes, the training/test split was 873/151. Segmentation quality was assessed on the held-out test set with Dice similarity coefficient (DSC), precision, recall, and Normalized Surface Dice (NSD) at a 2 mm tolerance. All of these metrics are reported per structure, aggregated over all 151 patients in the held-out test set. The trained model was then applied to the IUH cohort to generate the tumor and vessel masks, which are used downstream for the validation of the framework. This was done to automate the processing of the framework.

Shape analysis and statistics. For each patient, we computed the per-vessel encasement-angle profile and summarized it as $E_{\max}$ and AUEC for the SMA, CA, and SMV/PV, at contact thresholds $\tau \in \{1, 2, 3\}$ mm. As the preoperative resectability is an ordinal label, the primary analysis tested whether each metric increases monotonically across the resectable, borderline-resectable, and locally-advanced groups using the *Jonckheere-Terpstra* trend test (increasing alternative) [7, 17], with *Spearman's* ρ as effect size and *Kruskal–Wallis* test as a non-ordered secondary. Metastatic cases were excluded, as this is defined by distant spread rather than local encasement. τ=2 mm was as primary and report the remaining thresholds as sensitivity analyses. Significance was set at α=0.05.

4 Results

4.1 Tumor-Vessel Proximity Heatmap

Tumor-vessel proximity maps generated patient-specific, 3D proximity maps for the CA, SMA, and peripancreatic veins. Each peripancreatic vessel is colored by distance to the tumor, localizing the tumor-vessel interface in a single, view-independent image (Fig. 1 A,B): warm colors identify the longitudinal extent of the vessel in contact with the tumor, while cool regions indicate periadventitial

clearance, i.e., a larger distance between tumor and vessel, typically making tumor resection less complex in this region.

As the proximity map relies distances on automatically segmented or manually labeled surfaces, its fidelity is bounded by surface accuracy at millimeter scale of clinical tumor-vessel contact. For automation of the framework, on the held-out PanTS test set (n=151), segmentation performance was highest for SMA (DSC 0.891 ± 0.01) and veins (DSC 0.886 ± 0.02), followed by the pancreas (DSC 0.847 ± 0.02) and CA (DSC 0.798 ± 0.02). Lesion segmentation was more challenging (DSC 0.459 ± 0.05), (Table 1), due to isoattenuation, infiltrative margins, and the disproportionate Dice sensitivity to boundary errors in small lesions.

Rendering the 3D tumor-proximity map required a median of 3.3 s per case (IQR 2.6–3.7 s, range 0.3–6.9 s) with a peak memory footprint of 1.52 GB (AMD EPYC 9554 64-core processor and 377 GB RAM).

Table 1. Segmentation performance for the anatomical structures. Values are reported as mean ± confidence interval. Abbreviations: DSC, Dice Similarity Coefficient; NSD, Normalized Surface Distance; CA, Celiac Axis; SMA, Superior Mesenteric Artery.

Structure	DSC	Precision	Recall	NSD
CA	0.798 ± 0.016	0.827 ± 0.012	0.782 ± 0.018	0.920 ± 0.014
Pancreas	0.847 ± 0.017	0.861 ± 0.021	0.848 ± 0.015	0.863 ± 0.015
Pancreatic head	0.792 ± 0.026	0.806 ± 0.032	0.809 ± 0.019	0.803 ± 0.022
Pancreatic body	0.717 ± 0.032	0.771 ± 0.031	0.699 ± 0.034	0.724 ± 0.031
Pancreatic tail	0.782 ± 0.029	0.831 ± 0.025	0.765 ± 0.033	0.799 ± 0.029
SMA	0.891 ± 0.009	0.906 ± 0.012	0.883 ± 0.010	0.980 ± 0.005
Veins	0.886 ± 0.017	0.899 ± 0.015	0.883 ± 0.015	0.936 ± 0.015
Lesion	0.459 ± 0.054	0.686 ± 0.059	0.470 ± 0.059	0.426 ± 0.053

4.2 Encasement-Angle Profile

The continuous encasement-angle profile, $A(s)$, represents each branch of the vessel as an angle-versus-axial-position curve. This presents the location, circumferential extent, and longitudinal span of tumor contact, which is directly interpretable along the vessel (Fig. 1 C-H). In representative cases, the SMA profiles (Fig. 1 C, D) show contact confined to a discrete arterial segment. The celiac-axis profile in Fig. 1 E remains at 0°, indicating that no surface point lies within $\tau = 2\,\text{mm}$ of the tumor. In Fig. 1 F, contact is observed near the bifurcation origin, with an additional focal region along the mid-portion of the branch. The veins (SMV/PV) profiles (Fig. 1 G, H) demonstrate a broader and more extensive contact pattern. These continuous profiles reveal vessel-specific spatial patterns that cannot be captured by a single axial contact-angle measurement. Branch boundaries are explicitly marked at bifurcations. This allows encasement to be reported separately for each branch rather than averaged across a vascular confluence.

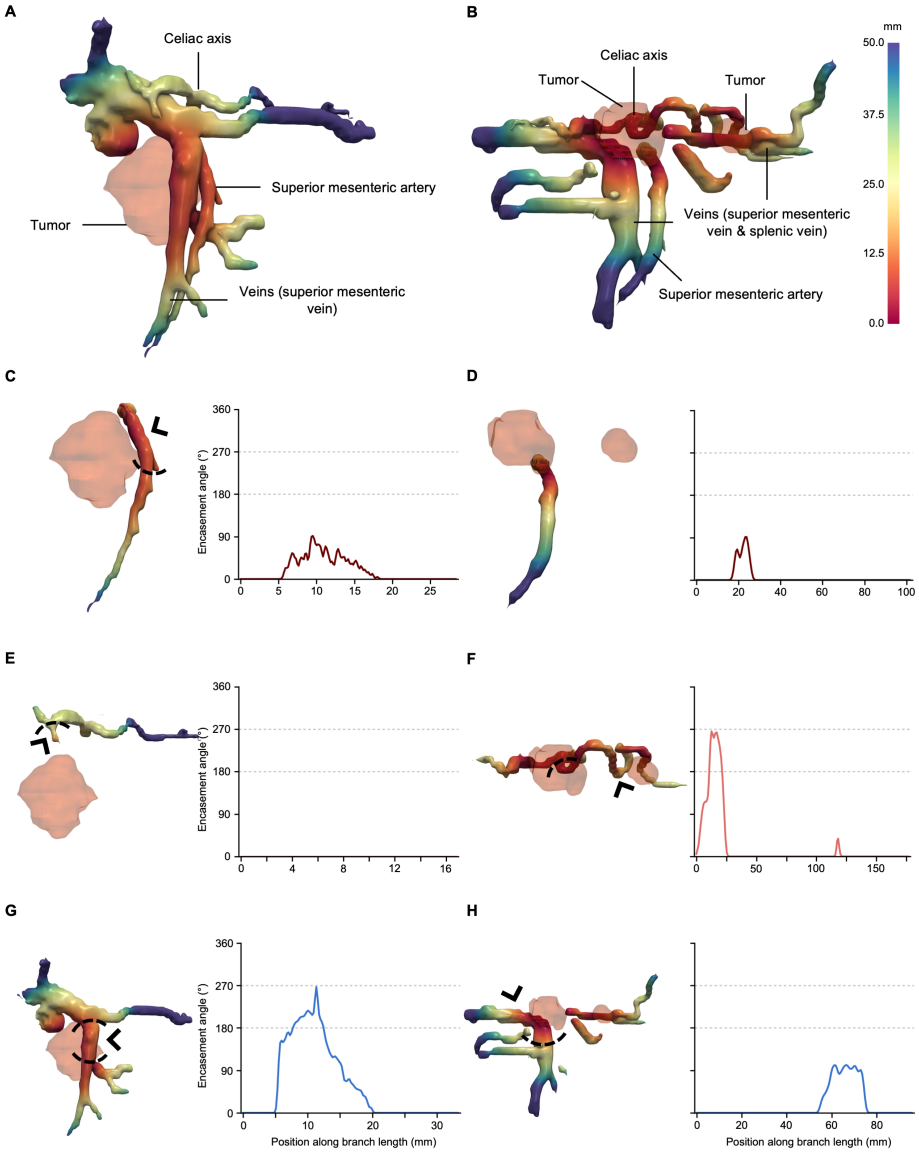

Fig. 1. The PanVasc framework on representative cases. (A, B) Tumor-vessel proximity map: each peripancreatic vessel surface is colored according to the distance to the nearest tumor-surface point. The color scale is capped at 50 mm, beyond which proximity is considered clinically irrelevant. **(C-H)** Encasement-angle profiles, $A(s)$, for the SMA (C, D), gastroduodenal artery (E), splenic artery (F), SMV (G), and PV (H) showing the circumferential extent of tumor contact within a threshold of $\tau = 2$ mm along each vessel branch. The dashed lines denote NCCN abutment-encasement thresholds. The celiac axis profile in E remains at 0°, as no surface point along this branch was within 2 mm of the tumor. Dashed arcs denote vessel bifurcations and the arrowhead identifies the branch corresponding to the displayed profile.

4.3 *AUEC* and E_{max} show significant monotonic increase across preoperative resectability classes

Across the 364 non-metastatic resected IUH patients (resectable n=266, borderline-resectable n=78, locally-advanced n=20), both arterial encasement summaries i.e., $AUEC$ and E_{max} increased with resectability stage for every vessel (contact thresholds evaluated: $1, 2, 3$ mm) (Supplementary Table 1 and 2). The Jonckheere-Terpstra trend was significant for all vessel-threshold combinations. For the CA at τ=1 mm, surface contact was near-absent in all groups (Fig. 2). Spearman correlations between the encasement summaries ($AUEC$ and E_{max})

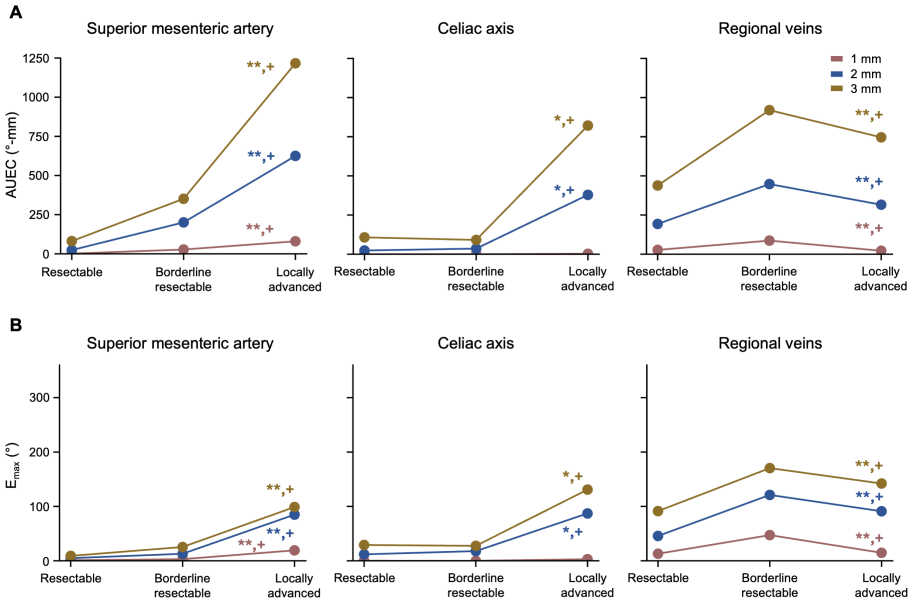

Fig. 2. Trend analysis and association of $AUEC$ and E_{max} with preoperative resectability classes. Mean (**A**) $AUEC$ (°-mm) and (**B**) $E_{\max}$ (degrees) for the SMA, CA, and regional veins across the resectable, borderline-resectable, and locally-advanced groups, at contact thresholds of 1, 2, and 3 mm. $*$ and $**$: Jonckheere-Terpstra trend across the ordered groups $p < 0.05$ and $p < 0.01$; $+$: positive significant correlation.

and the preoperative resectability classification were positive throughout. For SMA, $AUEC$ showed increasing correlations across thresholds $\rho = 0.17, 0.24, 0.26$ at $1, 2, 3$ mm, respectively, while venous $AUEC$ demonstrated a consistent correlation of $\rho = 0.22$ at all thresholds. Correlations for the CA were weaker, ranging from $\rho = 0.08$ to 0.12, and were not statistically significant at 1mm (Fig. 2 A).

The increase was *vessel-specific*. Arterial encasement rose sharply only into locally-advanced disease i.e., mean SMA $E_{\max}$ increased from 4.8° to 12.9° to

84.9° across the three groups at τ=2 mm. Similarly, mean CA $E_{\max}$ showed similar pattern at τ=2 mm (11.9° → 17.8° → 87.1°). Venous contact instead rose across the resectable-to-borderline resectable transition and did not increase further in patients with locally advanced disease (45.7° → 121.1° → 91.1°) (Fig. 2 B). $AUEC$ exhibited the same structure (Fig. 2 A). This observed double dissociation i.e., venous involvement marking the resectable/borderline boundary and arterial involvement the borderline/locally-advanced boundary, mirrors the vessel weighting of the NCCN resectability criteria [15]. The trend reflects an increasing prevalence and magnitude of contact across stages. Our framework reproduced this fully automatically from AI-based tumor and vessel segmentations alone.

5 Discussion

We present PanVasc, a shape-based framework that converts peripancreatic vasculature and pancreatic tumor into an interpretable description of vascular invasion of PDAC i.e., a 3D proximity map, a continuous per-vessel encasement-angle profile $A(s)$, and its scalar summaries $AUEC$ and $E_{\max}$. On an independent clinical cohort, arterial $AUEC$ and $E_{\max}$ increased monotonically with resectability stage for every vessel (Jonckheere-Terpstra $p < 0.05$; CA n.s. only at 1 mm), indicating the clinical relevance of our framework. The arterial encasement rose sharply only in patients with locally advanced disease while venous contact marked the resectable/borderline resectable transition.

This framework and the observed trends are relevant to preoperative resectability assessment, which relies on subjective mental reconstruction of the tumor-vessel interface from 2D axial slices and is known to vary between readers [8, 4]. Previous computational approaches have quantified vascular involvement from segmented CT images [19, 10]. PanVasc extends that and renders that interface explicit and quantitative. The metrics are continuous rather than categorical and offer a reproducible second reader and an objective substrate for longitudinal monitoring (e.g. restaging after neoadjuvant therapy).

Our study has a few limitations. The clinical analysis is single-center, retrospective, and restricted to resected patients, which truncates the high- encasement range and limits effect sizes. Moreover, because preoperative resectability grading itself incorporates vascular contact, our findings establish automated and reproducible *concordance* with expert staging, not independent prediction. Establishing clinical predictive utility will require prospective validation against endpoints such as intraoperative vascular involvement, margin status, and oncologic outcomes. Lastly, clinical-cohort metrics were based on predicted rather than verified segmentations. Lesion segmentation was the weakest component, and boundary errors may propagate downstream inaccuracies in the derived scalar summaries $AUEC$ and $E_{\max}$. Without reference annotations, this propagation cannot be quantified.

6 Conclusion

The PanVasc framework converts the complex 3D tumor-vessel interface into an explicit proximity map, a continuous vessel-specific encasement profile, and interpretable summary measures of peak and longitudinal contact. By preserving information that is otherwise compressed into a subjective categorical judgment, the framework provides a reproducible geometric basis for resectability assessment and vascular invasion. Future studies will focus on prospective multicenter validation against margin status, operative findings, treatment response, and survival.

Acknowledgments. FRK receives support from the German Federal Ministry for Research, Technology and Space BMFTR (GRAIL, 01ZU2505), the German Cancer Aid (AI-TME, 70116966), the German Cancer Research Center (CoBot 2.0), the Jung Foundation for Science and Research (Jung Career Advancement Award), the Evan and Sue Ann Werling Pancreatic Cancer Research Fund, the Central Indiana Corporate Partnership AnalytiXIN Initiative, and the Indiana Clinical and Translational Sciences Institute funded, in part, by the National Institutes of Health, National Center for Advancing Translational Sciences, Clinical and Translational Sciences Award (UM1TR004402). The content is solely the responsibility of the authors and does not necessarily represent the official views of the National Institutes of Health.

Ethics Statement. This study was carried out in accordance with the Declaration of Helsinki and its later amendments. The protocol was reviewed and approved by the institutional review board of Purdue University on February 7, 2024 (IRB-20231736). All patient data were de-identified prior to the analysis. Written informed consent was waived.

Disclosure of Interests. FRK declares ongoing advisory roles for Scopia AI, Canada, and has received research funding from Novartis. The other authors declare no competing interests.

References

1. Demir, I.E., Jäger, C., Schlitter, A.M., Konukiewitz, B., Stecher, L., Schorn, S., Tieftrunk, E., Scheufele, F., Calavrezos, L., Schirren, R., et al.: R0 versus r1 resection matters after pancreaticoduodenectomy, and less after distal or total pancreatectomy for pancreatic cancer. Annals of surgery **268**(6), 1058–1068 (2018)
2. Evans, D.B.: What makes a pancreatic cancer resectable? In: American Society of Clinical Oncology Educational book. American Society of Clinical Oncology. Annual Meeting. vol. 38, pp. 300–305 (2018)
3. von Fritsch, L., Duhn, J., Abdalla, T.S., Honselmann, K.C., Bolm, L., Braun, R., Kist, M., Lapshyn, H., Zeissig, S.R., Klinkhammer-Schalke, M., et al.: An r0 resection margin does improve overall survival after pdac resection–real-world evidence from 6.000 cases from the german cancer registry group. European Journal of Surgical Oncology **51**(6), 109693 (2025)

4. Giannone, F., Capretti, G., Hilal, M.A., Boggi, U., Campra, D., Cappelli, C., Casadei, R., De Luca, R., Falconi, M., Giannotti, G., et al.: Resectability of pancreatic cancer is in the eye of the observer: a multicenter, blinded, prospective assessment of interobserver agreement on nccn resectability status criteria. Annals of Surgery Open **2**(3), e087 (2021)
5. Halbrook, C.J., Lyssiotis, C.A., Di Magliano, M.P., Maitra, A.: Pancreatic cancer: Advances and challenges. Cell **186**(8), 1729–1754 (2023)
6. Isensee, F., Jäger, P.F., Kohl, S.A., Petersen, J., Maier-Hein, K.H.: Automated design of deep learning methods for biomedical image segmentation. arXiv preprint arXiv:1904.08128 (2019)
7. Jonckheere, A.R.: A distribution-free k-sample test against ordered alternatives. Biometrika **41**(1/2), 133–145 (1954)
8. Joo, I., Lee, J.M., Lee, E.S., Son, J.Y., Lee, D.H., Ahn, S.J., Chang, W., Lee, S.M., Kang, H.J., Yang, H.K.: Preoperative ct classification of the resectability of pancreatic cancer: interobserver agreement. Radiology **293**(2), 343–349 (2019)
9. Kaluba, B., Kuriyama, N., Nagata, M., Ito, T., Hayasaki, A., Fujii, T., Murata, Y., Tanemura, A., Kishiwada, M., Mizuno, S.: A severity-based tumor-superior mesenteric/portal vein interface grading criteria as a predictor of survival outcomes in pancreatic head ductal adenocarcinoma patients undergoing pancreaticoduodenectomy following neoadjuvant chemoradiotherapy. Annals of Gastroenterological Surgery **9**(4), 842–860 (2025)
10. Lao, Y., David, J., Fan, Z., Bian, S., Shiu, A., Chang, E.L., Sheng, K., Yang, W., Tuli, R.: Quantifying vascular invasion in pancreatic cancer—a contrast ct based method for surgical resectability evaluation. Physics in Medicine & Biology **65**(10), 105012 (2020)
11. Lermite, E., Sommacale, D., Piardi, T., Arnaud, J.P., Sauvanet, A., Dejong, C.H., Pessaux, P.: Complications after pancreatic resection: diagnosis, prevention and management. Clinics and research in hepatology and gastroenterology **37**(3), 230–239 (2013)
12. Li, W., Zhou, X., Chen, Q., Lin, T., Bassi, P.R., Chen, X., Ye, C., Zhu, Z., Ding, K., Li, H., et al.: Pants: The pancreatic tumor segmentation dataset. Advances in Neural Information Processing Systems **38** (2026)
13. Lorensen, W.E., Cline, H.E.: Marching cubes: A high resolution 3d surface construction algorithm. In: Seminal graphics: pioneering efforts that shaped the field, pp. 347–353 (1998)
14. McGuigan, A., Kelly, P., Turkington, R.C., Jones, C., Coleman, H.G., McCain, R.S.: Pancreatic cancer: A review of clinical diagnosis, epidemiology, treatment and outcomes. World journal of gastroenterology **24**(43), 4846 (2018)
15. National Comprehensive Cancer Network: NCCN clinical practice guidelines in oncology: Pancreatic adenocarcinoma, version 2.2026. `https://www.nccn.org/professionals/physician_gls/pdf/pancreatic.pdf` (2026), last accessed 22 June 2026
16. Taubin, G.: A signal processing approach to fair surface design. In: Proceedings of the 22nd annual conference on Computer graphics and interactive techniques. pp. 351–358 (1995)
17. Terpstra, T.J.: The asymptotic normality and consistency of kendall's test against trend, when ties are present in one ranking. Indagationes Mathematicae **14**(3), 327–333 (1952)
18. Wang, J., Ganjouei, A.A., Romero-Hernandez, F., Foroutani, L., Bahceci, D., Deranteriassian, A., Casey, M., Li, P.Y., Houshmand, S., Behr, S., et al.: A computer

vision algorithm to predict superior mesenteric artery margin status for patients with pancreatic ductal adenocarcinoma. Annals of Surgery **283**(5), 834–840 (2026)
19. Zhang, Y., Zhang, H., Yang, Y., Wu, C., Zhang, L., Xia, W., Wang, X., Zhang, X., Cao, L., Liu, M., et al.: A clinically validated 3d deep learning approach for quantifying vascular invasion in pancreatic cancer. NPJ Digital Medicine **9**(1), 79 (2025)